RESEARCH ARTICLE

Society For Biomaterials WILEY

Can strontium replace calcium in bioactive materials for dental applications?

Lauter Eston Pelepenko[1] | Marina Angelica Marciano[1] | Tamires Melo Francati[1] |
Gabriela Bombarda[1] | Thiago Bessa Marconato Antunes[1] | Francois Sorrentino[2] |
Richard A. Martin[3] | Elisa Boanini[4] | Paul Roy Cooper[5] |
Richard Michael Shelton[6] | Josette Camilleri[6]

[1]School of Dentistry of Piracicaba, State University of Campinas, Piracicaba, Brazil

[2]Mineral Research Processing, Meyzieu, France

[3]Aston Institute of Materials Research, Aston University, Birmingham, UK

[4]Department of Chemistry, "Giacomo Ciamician", University of Bologna, Bologna, Italy

[5]Department of Oral Science, Sir John Walsh Research Institute, University of Otago, Dunedin, New Zealand

[6]School of Dentistry, College of Medical and Dental Sciences, University of Birmingham, Birmingham, UK

Correspondence
Josette Camilleri, School of Dentistry, Institute of Clinical Sciences, College of Medical and Dental Sciences, University of Birmingham, 5, Mill Pool Way, Edgbaston, Birmingham B5 7EG, UK.
Email: j.camilleri@bham.ac.uk

Abstract

The substitution of calcium with strontium in bioactive materials has been promising but there has been some concern over the material instability and possible toxicity. The aim of this research was the synthesis and characterization of calcium and strontium substituted bioactive materials and assessment of interactions with local tissues and peripheral elemental migration in an animal model. A bioactive glass, hydroxyapatite and hydraulic calcium silicate with 50% or 100% calcium substitution with strontium were developed and the set materials were characterized immediately after setting and after 30 and 180-days in solution. Following subcutaneous implantation, the local (tissue histology, elemental migration) and systemic effects (elemental deposition after organ digestion) were assessed. The strontium-replaced silicate cements resulted in the synthesis of partially substituted phases and strontium leaching at all-time points. The strontium silicate implanted in the animal model could not be retrieved in over half of the specimens showing the high rate of material digestion. Tissue histology showed that all materials caused inflammation after 30 days of implantation however this subsided and angiogenesis occurred after 180 days. Strontium was not detected in the local tissues or the peripheral organs while all calcium containing materials caused calcium deposition in the kidneys. The tricalcium silicate caused elemental migration of calcium and silicon in the local tissues shown by the elemental mapping but no deposition of calcium was identified in the peripheral organs verified by the assessment of the digested tissues. Strontium can substitute calcium in bioactive materials without adverse local or systemic effects.

KEYWORDS
bioactivity, calcium-based materials, elemental migration, strontium-doping

1 | INTRODUCTION

Bioactive materials are used in various clinical procedures to replace bone and dental hard tissues. Bioactive biomaterials are created in such a way that elicits a specific biological response and avoids fibrous tissue layer formation. These biomaterials interact with the biological environment thus enhancing the biological response as well as the tissue/surface effect.

Bioglass is composed of 45 wt% SiO_2, 24.5 wt% CaO, 24.5 wt% Na_2O, and 6.0 wt% P_2O_5 and compared with soda-lime glasses, it contains less silica and higher amounts of calcium and phosphorus. This high ratio of calcium to phosphorus promotes the interaction of the material with bone and is thus used for biomedical applications as a bone replacement material.[1,2]

Strontium ions have been shown to stimulate bone formation and to inhibit osteoclastic resorption both *in vitro* and *in vivo*.[3,4] Sr-containing bioactive glasses have been shown to be effective for regenerative procedures[5] and also for bone repair and regeneration therapies, making them a promising material for bone substitution and therapeutic release of Sr ions. The replacement of Ca with Sr results in an expansion of the glass network owing to the larger ionic radius of Sr compared with Ca[6] and this alters the *in vitro* behavior of these glasses. By substituting Sr for Ca on a molar base, glass degradation and apatite formation can be increased, while providing release of Sr ions, which have been shown to stimulate bone formation.[3,4] In particular when fully substituting Ca with Sr, apatite formation was significantly enhanced.[7]

Although the substitution of Ca with Sr enhances ion release[8,9] and apatite formation, it does not necessarily benefit biological responses. Direct contact of murine fibroblasts with leachates from bioactive glasses containing strontium and magnesium reduced cell viability.[9] Sr-substituted bioactive glasses showed decreased bioactivity by blocking the active growth sites of calcium phosphate by Sr^{2+} and also reduced cell proliferation and alkaline phosphatase activity.[8] An indication of adequate biocompatibility of Sr-based glasses following direct contact with cells has been shown in other studies.[10]

Sr-substituted hydroxyapatite (HA) is also used for a variety of applications in orthopedic surgery. Since Sr^{2+} can replace Ca^{2+} in the HA structure, the degree of substitution influences HA solubility, which increases with increasing Sr content.[11] A 10% doped variant has been demonstrated *in vitro* to significantly increase levels of proliferation, alkaline phosphatase activity and collagen type I whilst down-regulating the production of interleukin-6, indicating a potential beneficial effect of strontium in the treatment of bone lesions and defects in the presence of osteoporotic bone.[12] In vivo Sr-HA has been successfully used for improving the posterolateral fusion rate in ovariectomized rats[13] as well as for restoring thoracolumbar vertebral body fractures.[14] The Sr doped HA has also been used to coat titanium implants to enhance osseointegration.[15,16] These material types are tailormade for specific applications in orthopedic surgery to modulate bone repair.

The success of Sr doping for medical applications has led to the use of Sr in bioactive glasses[17,18] and glass ionomer cements for dental use. Fuji IX (GC Europe, Leuven, Belgium) is a Sr-substituted glass ionomer cement used in restorative dentistry. Notably, Sr-based bioactive reinforced polyethylene composites may be suitable as obturation materials for endodontic treatment.[18] Bioactive glasses are also used in commercial formulations such as GuttaFlow Bioseal (Coltene, Langenau, Germany). In these formulations the $CaO-SiO_2-Na_2O-ZrO_2-P_2O_5$ bioactive glass is used in conjunction with a silicone matrix and also exhibited ion release and apatite formation in contact with physiological solutions.[19] GuttaFlow Bioseal induced limited inflammatory reactions at days 8 and 30 when implanted subcutaneously, with the initial inflammatory reactions subsiding within 30 days.[20] Furthermore, this material promoted cementoblast differentiation from human periodontal ligament stem cells in the absence of growth factors.[21]

Sr-based bioactive glasses have also been added to hydraulic cements to enhance bioactivity and anti-cariogenic potential.[17] The effect of Sr and Sr-based bioactive glasses on human dental pulp stem cells has also been investigated. Sr at specific doses significantly promoted proliferation, odontogenic differentiation and mineralization processes *in vitro* via the Ca sensing receptor pathway previously reported in osteoblast differentiation.[22] Understanding the actions of Sr will permit a more controlled application of its use in clinical practice.

Sr-doping in bioactive glasses clearly affects the leaching pattern of the material. Recent reports on the effects of leaching of metal ions from hydraulic calcium silicate cements have shown substantial amounts could be detected in tissue fluids and peripheral organs from dental cements.[23-26] Histological changes were quite marked in both liver and kidneys where the trace elements were deposited.[25,27] So far, the local and peripheral effects of Sr have not been investigated. The aim of this study was to assess Ca and Sr ion release and the deposition of these ions in peripheral organs of test animals for Sr doped bioactive glass, HA, hydraulic calcium silicate and two commercial glass ionomers.

2 | EXPERIMENTAL

2.1 | Materials and methods

A range of materials with Ca and Sr doping were evaluated. These included silicates, phosphates, bioactive glasses, and glass ionomers.

The following materials were assessed:

- Tricalcium silicate (TCS; Mineral Research Processing, Meyzieu, France)
- Tricalcium silicate doped with 50% or 100% strontium replacing the calcium (TCS-50, TCS-100; Mineral Research Processing, Meyzieu, France)
- Hydroxyapatite (HA; University of Bologna, Italy)
- Hydroxyapatite doped with 50% or 100% strontium replacing the calcium (HA-50, HA-100; University of Bologna, Italy)

- Bioactive glass (BG; Aston University, Birmingham, UK)
- Bioactive glass doped with 50% or 100% strontium replacing the calcium (BG-50, BG-100; Aston University, Birmingham, UK)
- Strontium free glass ionomer cement (Chemfil; Dentsply, Bensheim, Germany)
- Strontium doped glass ionomer (Fuji IX; GC Europe, Leuven, Belgium)

The TCS and HA with variants were combined with distilled water. The bioactive glass and Sr-doped variants were mixed with 2% sodium alginate after which they were covered with a filter paper soaked in 1% calcium chloride to allow cross-linking of the sodium alginate. The sodium alginate was used as a vehicle for the bioglass as it is resorbable, naturally derived and already has approval for use in humans. The liquid to powder ratios used are shown in Table 1. The glass ionomers were mixed according to the manufacturer's instructions.

2.1.1 | Material synthesis

The tricalcium silicate cement was manufactured using a sol gel method followed by sintering. Calcium nitrate and tetraethoxy silane were combined and hydrolysis and poly-condensation of metal alkoxides occurred leading to formation of particles undergoing agglomeration. The strontium-doped variants were synthesized by combining analar grade strontium carbonate (Merck, Darmstadt, Germany) to the calcium silicate using the formula $(Ca_x, Sr_{(1-x)})_3 Si O_5$ with a variation $X = 0$ for 100% substituted and $X = 1$ for pure tricalcium silicate. After mixing, the product was sintered at 1200°C for 2 h, cooled and ground to a fine powder. The powder was then mixed with water to obtain a slurry and pelletized and fired at 1550°C for 2 h.

Synthesis of HA nanocrystals was carried out by dropwise addition of 0.65 M $(NH_4)_2HPO_4$ (50 ml) into 1.08 M $Ca(NO_3)_2 \cdot 4 \ H_2O$ (50 ml) solution at pH adjusted to 10 with NH_4OH. The reaction was undertaken at 90°C while stirring in a N_2 atmosphere, the precipitate remained under the same conditions in contact with the mother solution for 5 h. The strontium-doped variants HA-50 and HA-100 were synthesized by addition of $(NH_4)_2HPO_4$ into a 50 ml solution containing 0.54 M $Ca(NO_3)_2 \cdot 4 \ H_2O$ and 0.54 M $Sr(NO_3)_2$ or only 1.08 M $Sr(NO_3)_2$, respectively.

The bioglass and Sr-substituted bioactive glasses were prepared using the melt-quenching technique. The glasses were synthesized from high purity SiO_2 (Alfa Aesar, 99.5%), Na_2CO_3 (Sigma-Aldrich, 99.5%), $NH_4H_2PO_4$ (Sigma-Aldrich, 99.5%), $CaCO_3$ (Alfa Aesar, 99.95–100.05%), and/or $SrCO_3$. The precursors were thoroughly mixed before transferring into a 90% platinum / 10% rhodium crucible. The reagents were heated to 1450°C with a heating rate of 10°C min^{-1} and held for 90 min before quenching into graphite molds.

2.1.2 | Material characterization

Material characterization was performed on the powders, set materials and the set materials after immersion in Hank's balanced salt solution (HBSS; H6648, Sigma Aldrich, Gillingham, UK) for 30 and 180 days. The HBSS included glucose: 1.0 g/L and $NaHCO_3$: 0.35 g/L and was free of phenol red, calcium chloride and magnesium sulfate.

Powder diffractometry

Phase analysis of the unhydrated powders was performed using a Bruker D8 Advance diffractometer (Bruker ASX, Billerica, MA, USA) with a Cu tube and Bragg–Brentano geometry. The specimen was placed over a sample holder and the X-ray tube was set to rotate between 10° and 50° spinning at 15 revs per min with a step size of 0.02° and 0.6 steps/s. Phase identification was accomplished using a search-match software utilizing ICDD database (International Center for Diffraction Data, Newtown Square, PA, USA).

The structural analysis of the crystalline samples were collected using a PANalytical-X'Pert PRO powder diffractometer equipped with a fast X'Celerator detector, counting for 1200 s at each 0.033° (2θ). Cell parameter calculations were processed with the Rietveld routine of the HighScore Plus software (PANalytical). The line broadening of the 002 and 310 reflections were used to evaluate the length of the coherent domains (τ_{hkl}) along the crystallographic c-axis and along a direction perpendicular to it. τ_{hkl} values were calculated from the widths at half maximum intensity using the Scherrer equation.[12]

Characterization of set materials

The materials were mixed at the defined liquid/powder ratios shown in Table 1. The mixture was placed in molds of 10 mm diameter and 2 mm high and were allowed to set at 100% humidity for 24 h. Samples ($n = 3$) were removed from the molds and characterized using scanning electron microscopy and energy dispersive spectroscopy. The specimens were embedded in epoxy resin (Epoxyfix, Struers, Ballerup, Denmark) and polished using ascending grids of diamond disks and polishing cloths with diamond pastes. Specimens were then mounted on aluminum stubs held in place with carbon tape and sputter coated with gold for electrical conductance. Specimens were viewed using a scanning electron microscope (Zeiss MERLIN Field Emission SEM, Carl Zeiss NTS GmbH, Oberkochen,

TABLE 1 Materials tested and their liquid/powder ratios

Material	Liquid/powder ratio
TCS	0.35
TCS-50	0.35
TCS-100	0.35
HA	0.65
HA-50	0.80
HA-100	0.65
BG	0.35
BG-50	0.35
BG-100	0.35
Chemfil	Manufacturer instructions
Fuji IX	Manufacturer instructions

Germany) at an accelerating voltage of 20 kV. The material microstructure was assessed using the back-scatter detector to obtain elemental contrast. Images at a range of magnifications (×500, ×1K, ×2K) were obtained. Energy dispersive spectroscopy was performed to assess the elemental composition.

Two other batches of test materials were weighed and placed in 5 ml HBSS. After 30 and 180 days the set materials were retrieved from the solution, placed in a desiccator with silica gel and soda lime to dry the material and avoid environmental contamination. After drying for 24 h samples were characterized using X-ray diffraction analysis and the leachates were assessed with inductively coupled plasma (ICP).

For X-ray diffraction analysis, after 30 and 180 days, the set materials were removed from solution, desiccated and ground to fine powders using an agate mortar and pestle. The phase analysis was performed using a Bruker D8 Advance diffractometer (Bruker ASX, Billerica, Ma, USA) with a Cu tube and Bragg–Brentano geometry. The specimen was placed over a sample holder and the X-ray tube was set to rotate between 10° and 50° spinning at 15 revs per min with a step size of 0.02° and 0.6 steps/s. Phase identification was accomplished using a search-match software utilizing ICDD database (International Center for Diffraction Data, Newtown Square, PA, USA).

Leachates of the materials were assessed after 30 and 180-day immersion in HBSS with blank HBSS used as the control. The leachates were filtered, diluted in 1:20 and acidified. The calcium and strontium ion leaching were assessed using optical emission spectrometry (ICP-OES, Perkin Elmer, Optima 8000). The leaching was calculated in micrograms per gram taking into consideration the volume of the solution and the specimen weight.

2.1.3 | Assessment of local tissue inflammatory response and elemental migration

The local tissue tolerance was assessed by histological analysis of the tissues in contact with the test materials after subcutaneous implantation. The elemental migration was assessed by ICP-OES in peripheral organs after 30 and 180-day implantations. All animal experiments complied with the ARRIVE guidelines and were carried out in accordance with the NIH Guide for Care and Use of Laboratory Animals guidelines.[28]

Materials were implanted in the subcutaneous tissues of male Wistar rats (*Rattus norvegicus*) weighing approximately 370 g. Ethical approval for animal use was obtained by the Animal Use Ethical Committee of the State University of Campinas (CEUA, FOP/UNICAMP number 4862–1/2018). The sample size was calculated using the Gpower 3.0 software,[29] considering a power test of 0.8.[30] Five animals per material type per test period were used. The negative control (n = 3) included animals not exposed to any surgery.

For the surgical procedures, the animals were anesthetized with a combination of ketamine and xylazine (Vet Brands Int, Miramar, Florida, USA) (0.05 ml/100 g) and the dorsal region was trichotomized and cleaned with iodine. A longitudinal incision was made using a #15

scalpel blade and two cylindric implants (4 mm × 2 mm) weighing approximately 0.035–0.05 g of the same freshly mixed material were placed – one sample in each surgical pocket side, 10 mm distant from the incision. The edges of the incisions were sutured with silk thread 4.0 and dipyrone was administrated at a dose of 100 mg/kg. The animals were kept at all times grouped according to the received exposure to avoid contamination between groups. Blood was extracted after 30, 60, 90, 120, and 180 days and assessed for calcium, strontium, silicon, and phosphorus by ICP-OES.

After 30 and 180 days, all animals were sacrificed with a lethal dose of ketamine/xylazine combination. The tissues around the material implants were dissected; the right side tissue segment was used for histological analysis and the left side tissue used for ICP-OES local analysis. Samples for elemental analysis were collected from intracardiac blood and from the liver, brain, and kidney.

Histological assessment

For the histological processing of the subcutaneous tissue, each sample was separately fixed in 10% formalin for 48 h and washed under running water for another 24 h. In sequence, all specimens were paraffin-embedded and sectioned in 5-μm thickness slices using a microtome (Leica RM 2155, Nussloch, Germany). The slices were deparaffinized with xylene for 10 min at 60°C and dehydrated with an ethanol sequence for the H&E staining. A light microscope system (Leica DM 5000 B Leica, Milan, Italy) connected to a camera (Leica DC 300 F Leica, Milan, Italy) was used for imaging and descriptive analysis of the inflammatory infiltrate around implants.

Elemental migration assessment

The tissues surrounding the second material implant were isolated, fixed in glutaraldehyde, dried with ascending grades of ethanol, critically point dried, sectioned transversely and mounted on aluminum stubs prior to coating with gold. The tissues were viewed using scanning electron microscopy as previously described at low magnification in order to visualize the skin and subcutaneous layer. Elemental maps for calcium, silicon, phosphorus, and strontium were acquired.

The tissue samples from the liver, brain and kidneys were weighed, standardized to 0.2 g, then digested using a closed digestion tube (Ultrawave Milestone, Shelton, CT, USA) using 6 ml of 20% nitric acid (Sigma Aldrich - Merck, Germany) redistilled by a sub-boiling process and 2 ml 30% hydrogen peroxide (Sigma Aldrich - Merck, Germany). The microwave cycle used a constant power of 1000 W and pressure of 20 bar for 5 min at 160°C, 2 min at 160°C, 5 min at 170°C, and 15 min at 170°C for all the digestions. Along with each digestion cycle, one blank was obtained using the same cycling conditions and with the same added reagents, but containing no sample, to assess the specific quality standard of the sample-round. The calibration curves for the readings were prepared using calibration standards with concentrations of 1000 ± 3 μg/mL prepared in 2% nitric acid (HPS, High Purity Standards, North Charleston, SC, USA) for each assessed ion. The strontium, silicon, calcium, and phosphorus mass fractions were assessed for the digested liver, brain and kidney and
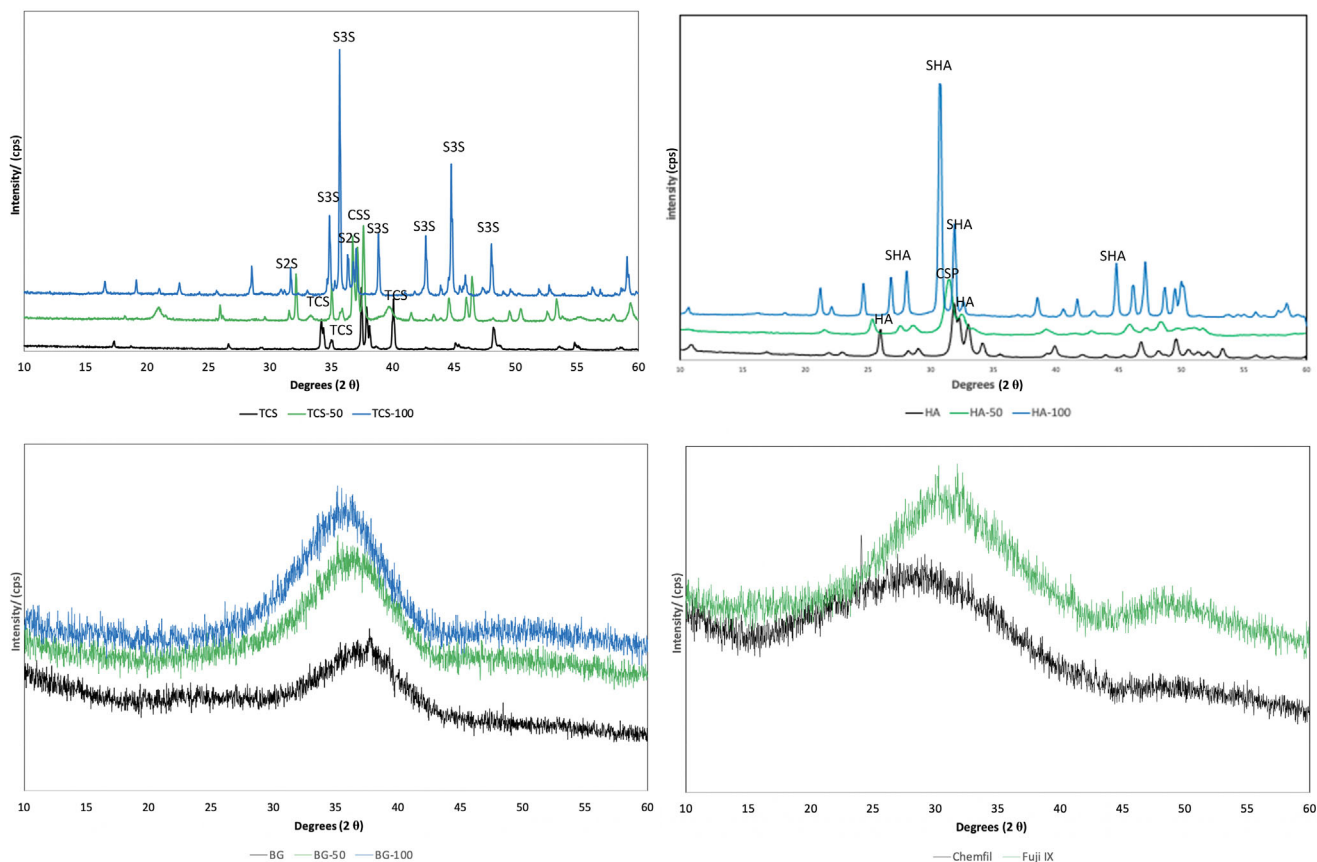
FIGURE 1 X-ray diffraction plots of test powders with and without strontium doping showing the main phases present. The bioactive, strontium-doped bioactive glass and the glass ionomers were amorphous with no detectable peaks. CS, $Ca_{2-x}Sr_xSiO_4$ (ICDD: 98–008-2997); CSP, calcium strontium phosphate (ICDD 34–0479); HA, hydroxyapatite (ICDD: 9–432); SHA, strontium-hydroxyapatite (ICDD 33–1348); TCS, tricalcium silicate (ICDD: 00–049-0442); S3S: $Sr_3 Si O_5$ (ICDD: 98–041-8933); S2S: $Sr_2 Si O_4$ (ICDD: 00–039-1256) ($n = 3$)

also for the intra-cardiac blood and expressed in nanograms per gram (ng/g). The filtered water, feed and wood shavings used for the animals' maintenance were also analyzed.

2.2 | Statistical analysis

The data normality was assessed Shapiro–Wilk test and comparisons according to data distribution used one-way ANOVA or Kruskal-Wallis followed by Tukey' or Dunn's test according to the type of comparison. The material characterization was performed in triplicate. The animal experiments and ensuing tests were completed with five replicates.

3 | RESULTS

3.1 | Material characterization

Powder diffractometry
The XRD scans of the powders are shown in Figure 1. The TCS scan showed a fully crystalline structure with definite peaks for tricalcium silicate (ICDD: 00–049-0442). Peaks were identified at 34, a bifid

TABLE 2 (A) Cell parameters of HA, HA-50, and HA-100, which indicate strontium substitution to calcium in the crystalline structure of hydroxyapatite. (B) Coherent lengths (h k l) of the perfect crystalline domains in the direction normal to 002 and to 310 planes calculated using the Scherrer method

(A)		
Sample	a-axis (Å)	c-axis (Å)
HA	9.448 (2)	6.895 (2)
HA-50	9.60 (5)	7.15 (10)
HA-100	9.779 (4)	7.289 (4)
(B)		
Sample	τ_{002} (Å)	τ_{310} (Å)
HA	473 (6)	232 (4)
HA-50	111 (2)	72 (1)
HA-100	492 (4)	368 (9)

peak at 37 and a peak at 40° 2θ. The 50% Sr-doped cement showed a mixture of phases with $Ca_{2-x}Sr_xSiO_4$, a Ca_2SiO_4 partially substituted in strontium (ICDD: 98–008-2997) showing peak shifts caused by the strontium substitution. The TCS-100 exhibited peaks for two
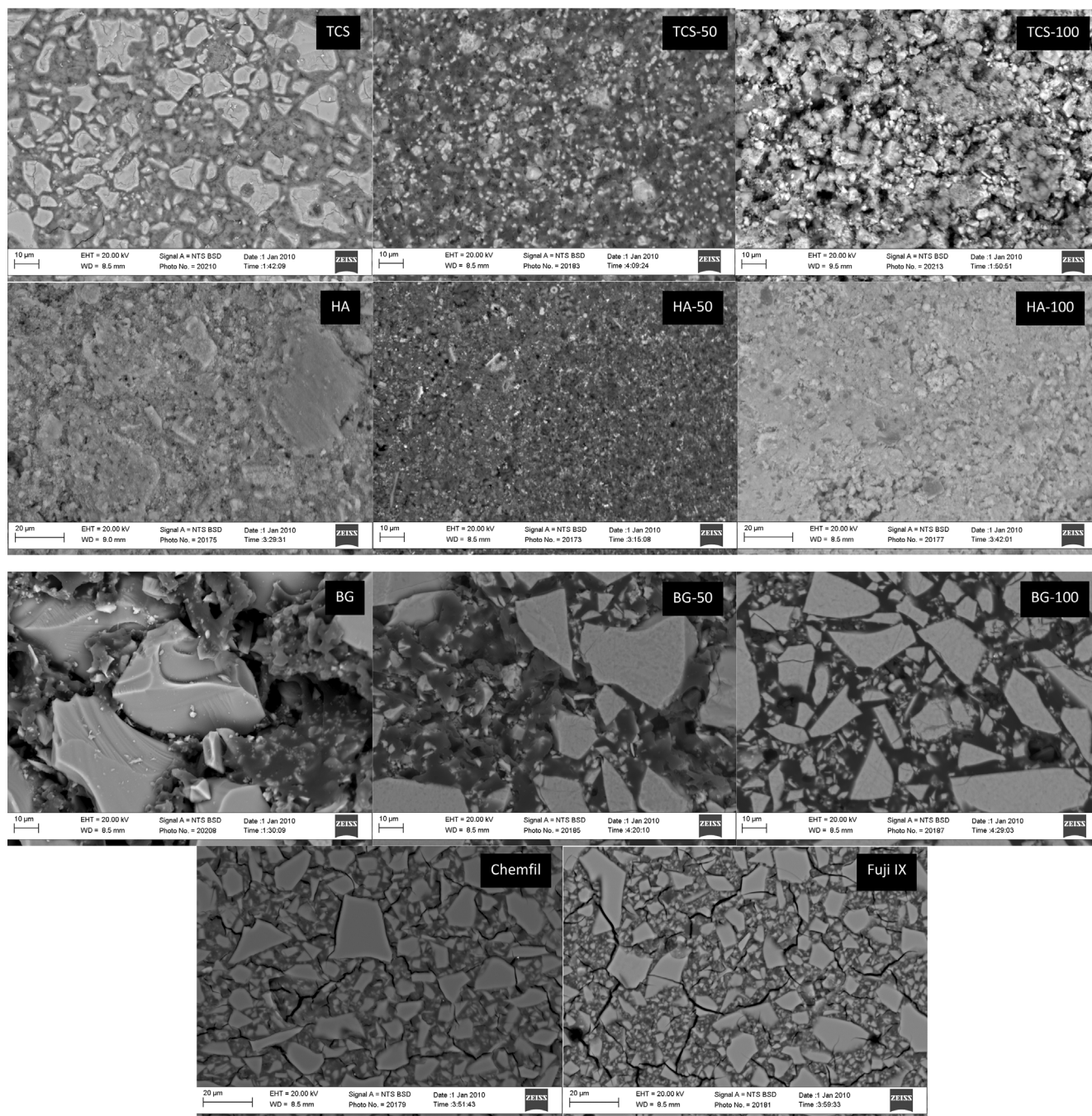
(a)

FIGURE 2 (A) Back scatter scanning electron micrographs of the different test materials showing their microstructure 2 K × magnification (n = 3). (B) EDS analysis of the materials to show the main elemental composition (n = 3)

strontium silicates $Sr_3 Si O_5$ (ICDD: 98–041-8933) and $Sr_2 Si O_4$ (ICDD: 00–039-1256).

X-ray diffraction of the HA sample showed a crystalline structure corresponding with pure hydroxyapatite (ICDD: 9–432). Sample HA-50 showed peaks of calcium strontium phosphate (ICDD 34–0479) and sample HA-100 exhibited peaks corresponding with strontium-hydroxyapatite (ICDD 33–1348). Increasing Sr substitution for Ca in the HA structure provoked a shift of XRD peaks toward lower angles, due to an increase in the cell parameters, in agreement with the

increasing mean dimensions of the cation. The values of cell parameters calculated for different samples are reported in Table 2 and data indicated the regular incorporation of the ion inside the crystal lattice of HA. The effect of Sr on crystallinity changed with composition: a partial Sr replacement with Ca induced a decrease in the coherent length of the perfect crystalline domains and disturbed the shape of the crystals. In fact, the XRD pattern of HA-50 displayed very broad peaks when compared with HA and HA-100, where crystallinity increased. Table 2 shows the crystal sizes of the different samples
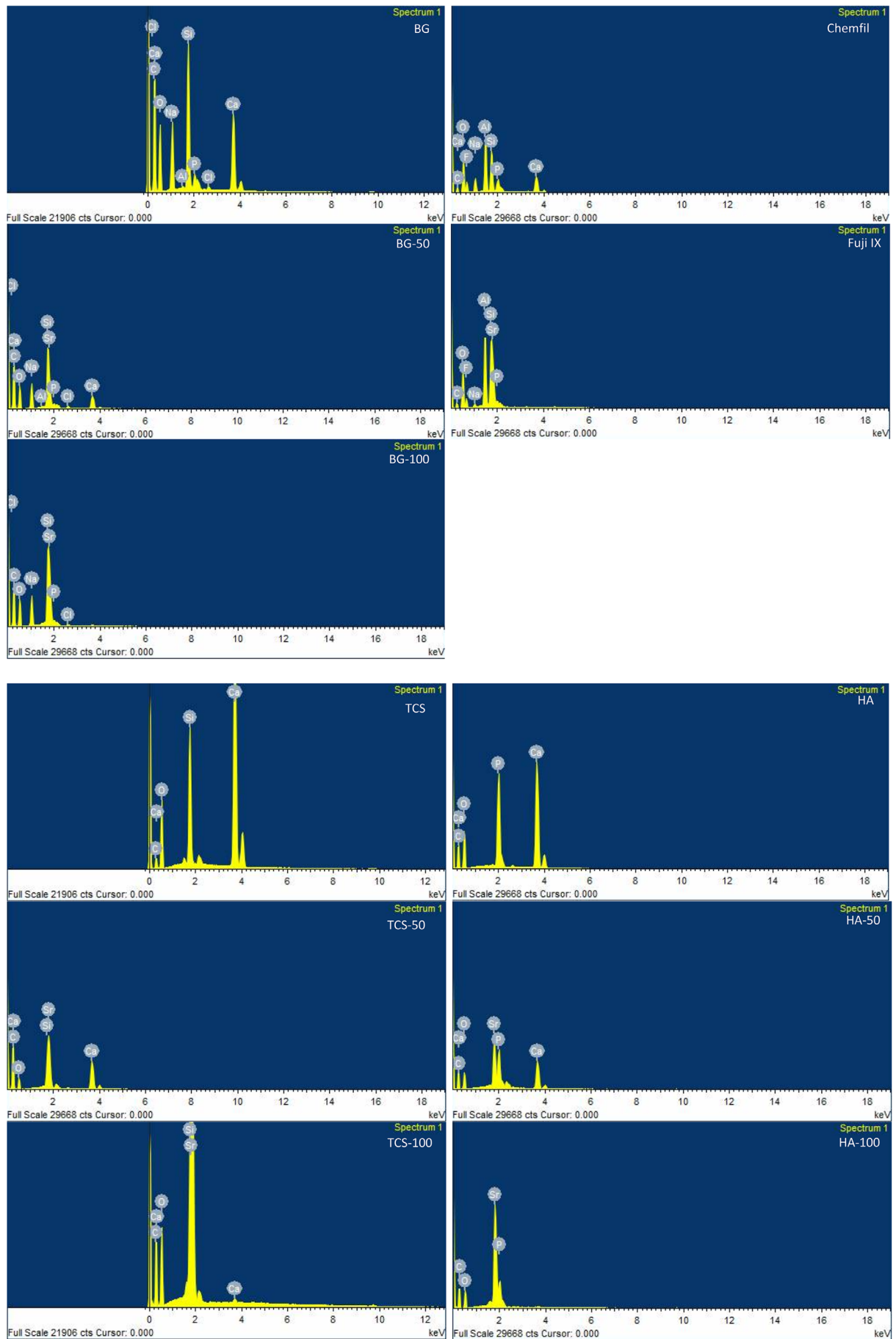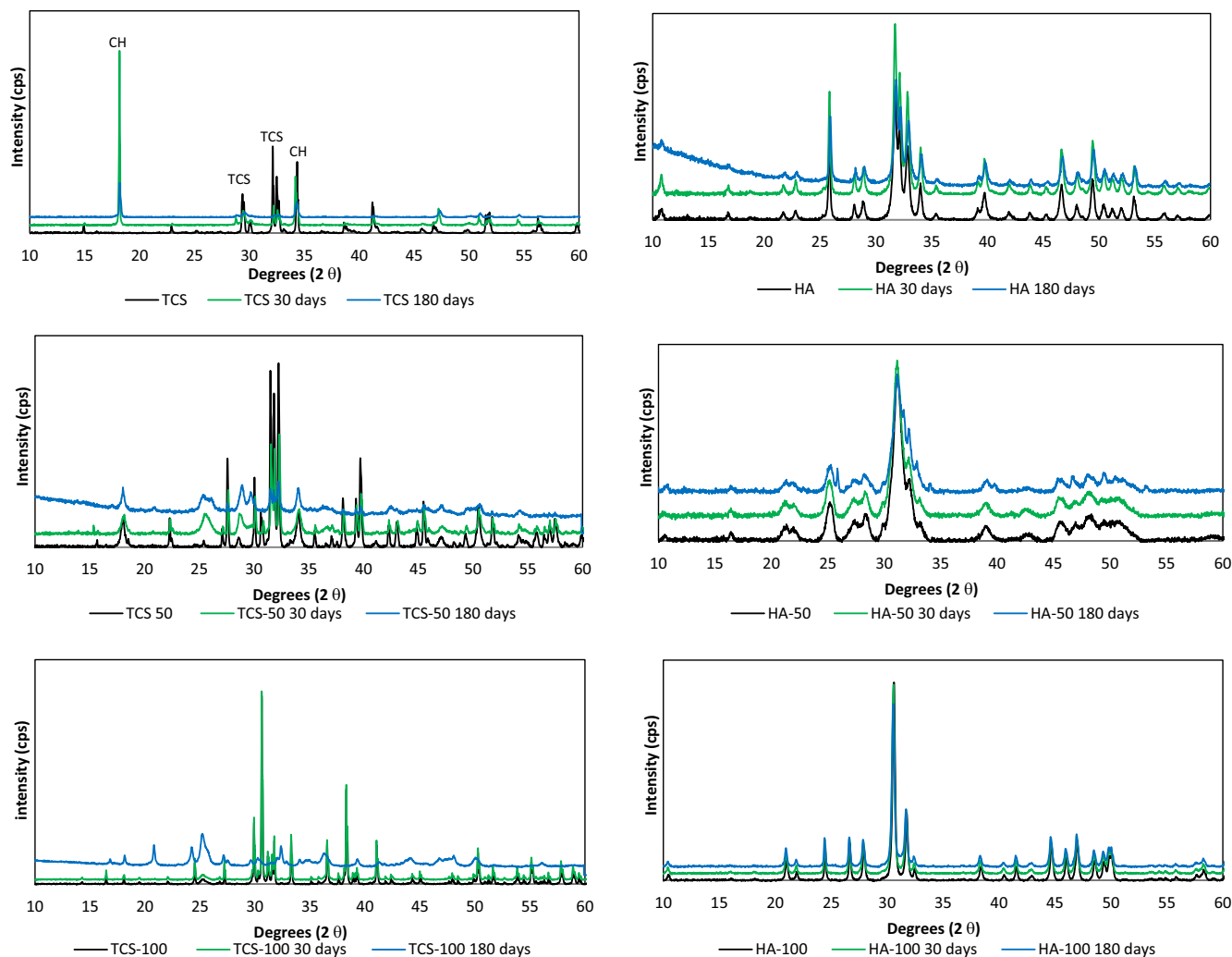
FIGURE 2 (Continued)

FIGURE 3 X-ray diffraction plots of test materials and strontium doped versions showing the main phases present. The TCS variants exhibited phase changes throughout the 180 days while HA was stable. The BG exhibited some crystalline changes which were more marked in the BG-100 after 180 days. CH, calcium hydroxide; TCS, tricalcium silicate; ($n = 3$)

calculated using the Scherrer formula along the direction of crystallographic c-axis (τ_{002}) and a perpendicular direction (τ_{310}).

The bioglass, Sr-doped bioactive glass and the commercial glass ionomers had an amorphous structure with no peaks identifiable following XRD analyzes (Figure 1).

Scanning electron microscopy and energy dispersive spectroscopy

Scanning electron micrographs showing the material microstructure and the EDS analysis data of the test materials are provided in Figure 2A,B, respectively. The particle size distribution of the three material types and the commercial glass ionomers was variable. Bioactive glass samples demonstrated the largest particle size with the glass particles being approximately 30 μm in size followed by the commercial glass ionomers (15–20 μm) with the HA and Sr doped HA having the smallest particle sizes (<5 μm). The replacement of Ca with Sr changed the material microstructure completely. The Sr doping resulted in smaller particle sizes and also an increase in opacity of the materials. The

tricalcium silicate material exhibited peaks for Ca, Si and O. The Sr replacement reduced the Ca peak until total replacement with Sr in the TCS-100 (Figure 2B). The HA exhibited peaks for Ca and P, whereas sample HA-50 showed the presence of Ca, Sr and P and in HA-100 Sr replaced all the Ca (Figure 2B). The EDS analysis (Figure 2B) for bioglass showed peaks for Ca, Si, O, and Na with minor peaks for P and Cl. The Na and Cl originated from the sodium alginate with additions of calcium chloride used for the cross linking. An Al peak was also observed. This could have resulted from the aluminum stub. The Ca peak diminished in intensity in the 50% Sr substituted bioactive glass and this was removed completely in the 100% Sr replaced glass. Chemfil showed elemental peaks for Ca, P, Al, Si, Na and F. Fuji IX did not contain Ca and exhibited peaks for P, Si, Na, Al, and Sr (Figure 2B).

Phase analysis of set materials

The XRD scans of the 30 and 180-day aged materials superimposed on the XRD scans of the powders is shown in Figure 3. The
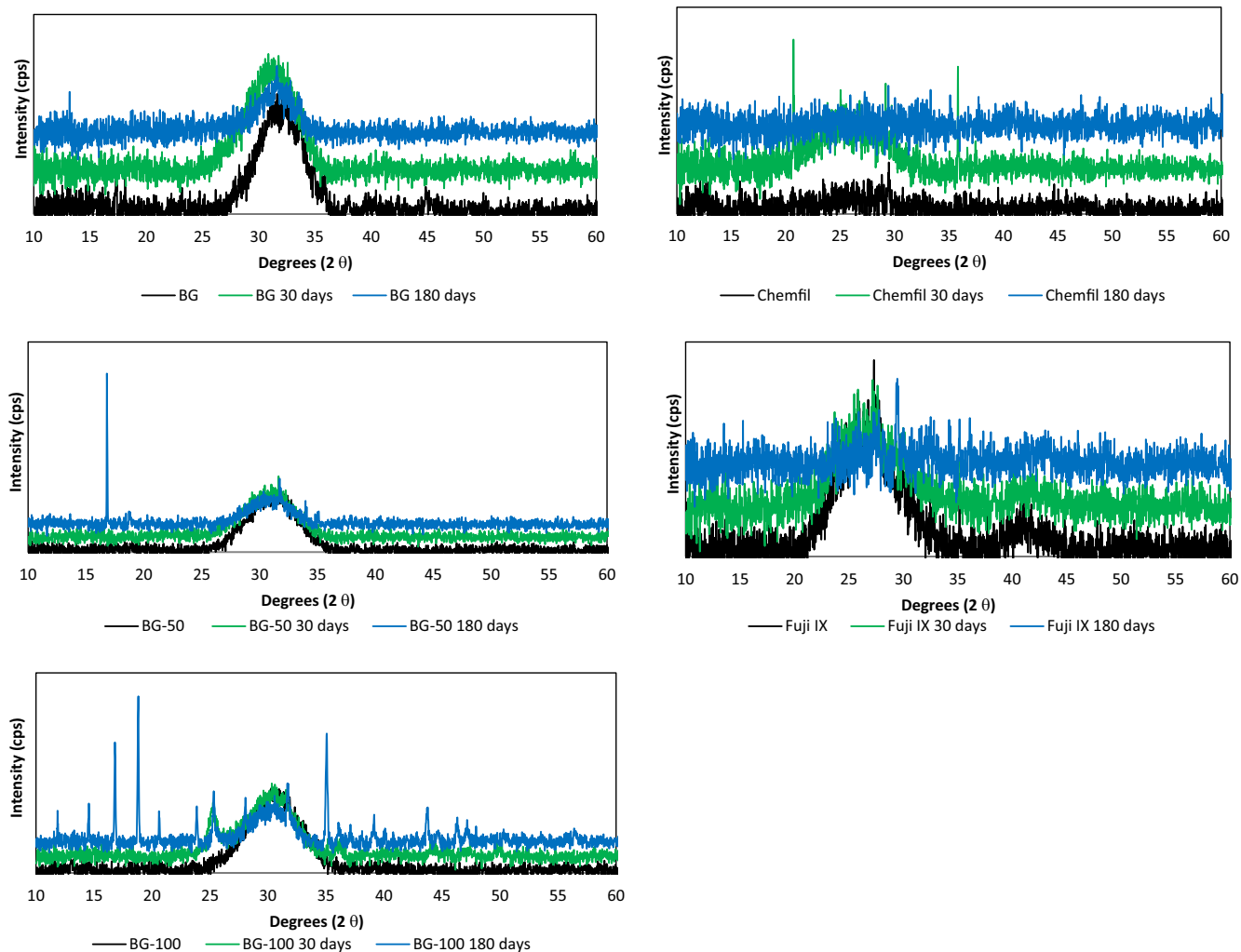
FIGURE 3 (Continued)

TABLE 3 Leaching of calcium and strontium from the test materials after 30 and 180 days (mean and standard deviation $n = 3$)

	Ion leaching mg/g			
	Ca		Sr	
Material	30 days	180 days	30 days	180 days
TCS	1997.0 ± 252.9	2581.8 ± 194.2	BDL	BDL
TCS-50	233.0 ± 19.2	242.1 ± 11.3	11,955.7 ± 70.5	23,297.7 ± 990.7
TCS-100	6.4 ± 4.4	27.1 ± 2.1	15,352.4 ± 1402.0	22,485.6 ± 1673.8
HA	2.1 ± 1.6	76.9 ± 27.4	BDL	BDL
HA-50	0.8 ± 0.2	4.4 ± 2.6	16.0 ± 0.5	9.0 ± 2.1
HA-100	BDL	BDL	4.7 ± 0.3	23.5 ± 9.7
BG	15.0 ± 4.5	27.3 ± 3.9	BDL	BDL
BG-50	14.6 ± 4.6	31.9 ± 4.3	91.0 ± 9.8	221.3 ± 68.9
BG-100	BDL	BDL	270.8 ± 7.2	699.0 ± 84.5
Chemfil	15.8 ± 6.4	59.0 ± 11.9	BDL	BDL
Fuji IX	10.0 ± 12.8	63.0 ± 10.7	379.8 ± 33.5	846.5 ± 165.8

Abbreviation: BDL, below detection limits.

(a)

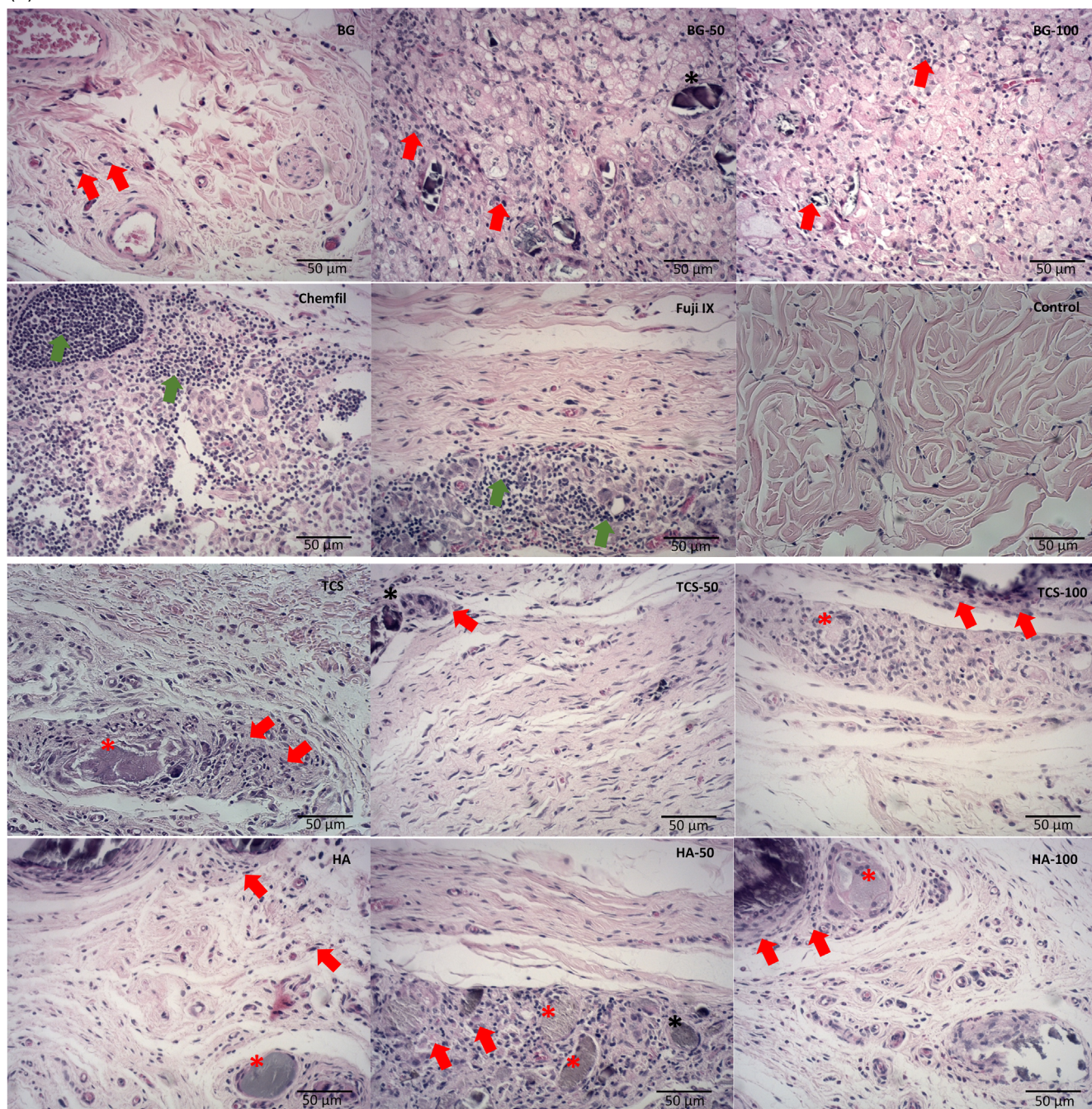**FIGURE 4** (A) Hematoxylin & eosin-stained representative light micrographs (40×), after 30 days, of the subcutaneous tissue adjacent to the material implant showing inflammatory cell infiltrate (red arrows) for all materials and its strontium replacements in different levels. In the Fuji and ChemFil samples an intense inflammatory cell concentration (green arrows) could be observed, and normal histology was observed in the negative control samples. Besides, detached material fragments (*) could be observed interposed within the connective tissue surrounded by a characteristic inflammatory chronic cell infiltrate representing a granulomatous foreign-body reaction ($n = 5$ for each material at different time points). (B) Hematoxylin & eosin-stained representative light micrographs (40×), after 180 days, of the subcutaneous tissue adjacent to the implant showing a mild inflammatory cell infiltrate with collagen fibers (arrows) indicating potential tissue repair. Tissue disorganization (#) was observed for all the 100% strontium-doped groups, Fuji, and ChemFil. Moderate angiogenesis and mild fibrosis (§) were also evident in this period of analysis for the test groups, whereas a more normal histology was observed for the negative control. ($n = 5$ for each material at different time points)

tricalcium silicate hydrated exhibited a calcium hydroxide peak at 18°θ. The tricalcium silicate peaks at 29, 32 and 34 °θ were diminished in intensity indicating the reaction and formation of calcium silicate hydrate. By 180 days only the calcium hydroxide peaks at 18 and 34 °θ were present indicating full hydration of the TCS. The TCS-50 exhibited a reduction in peak height of the tricalcium silicate
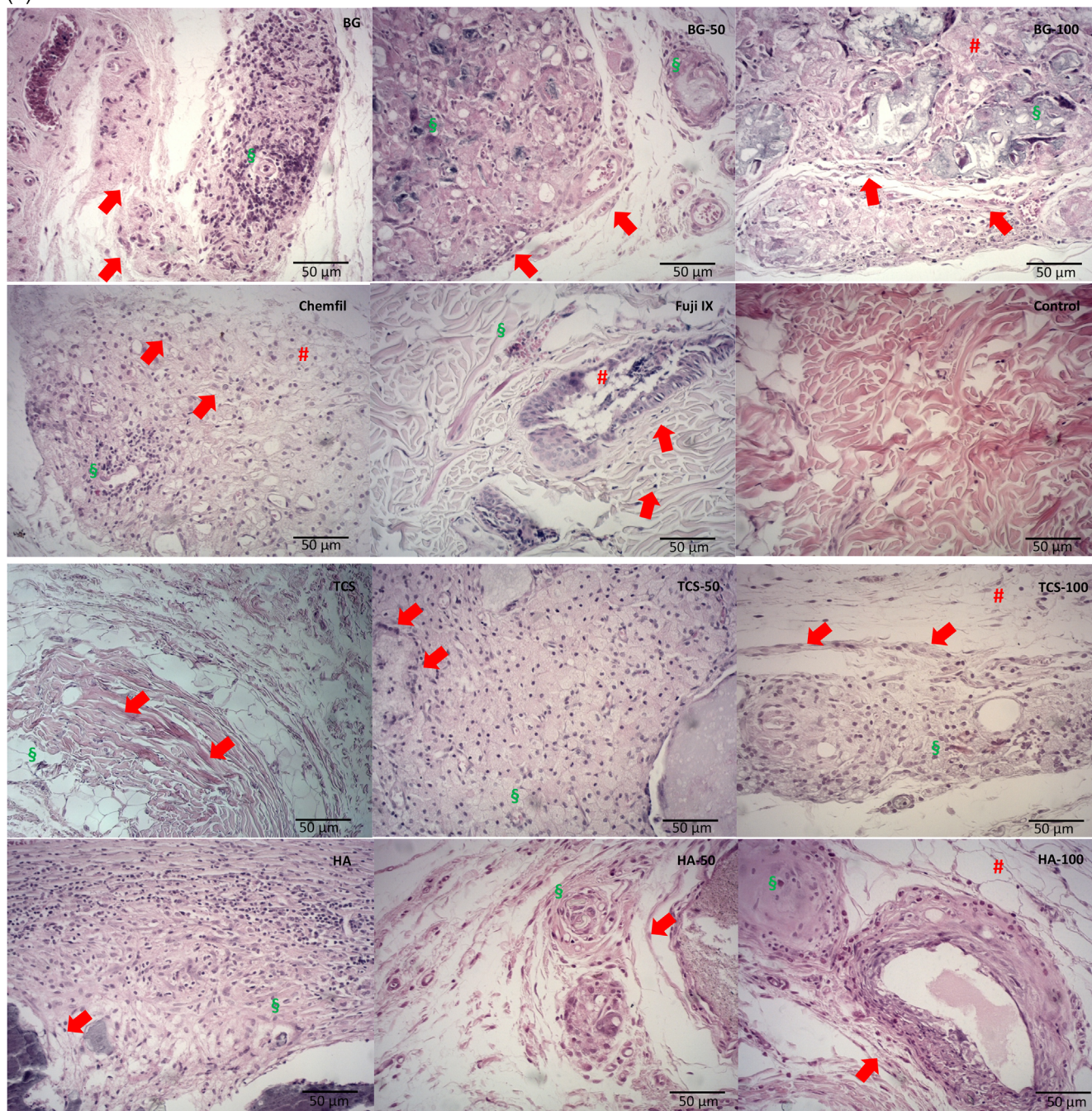
(b)

FIGURE 4 (Continued)

peaks at 32 and 34 °θ but no formation of calcium hydroxide was demonstrated. The TCS-100 exhibited a slow conversion from a fully crystalline phase to being mostly amorphous by 180 days. These changes were not immediate as after the 30-day period, the strontium silicate remained mostly unconverted.

The HA (Figure 3) and the Sr-doped materials of HA-50 and HA-100 did not exhibit any phase changes over the entire testing period. The bioactive glass BG (Figure 3) was amorphous with no specific peaks. The BG-100 showed the formation of a peak at 25 °θ

indicating the formation of a crystalline phase after 30 days and various other peaks after 180 days. No changes were observed in the commercial glass ionomer cements (Figure 3).

Leachate analysis

The leaching pattern of the test cements in HBSS is shown in Table 3. The levels of Ca and Sr leached varied between the material types. The highest levels for both elements was shown by tricalcium silicate, followed by the bioactive glasses. The commercial glass ionomers and
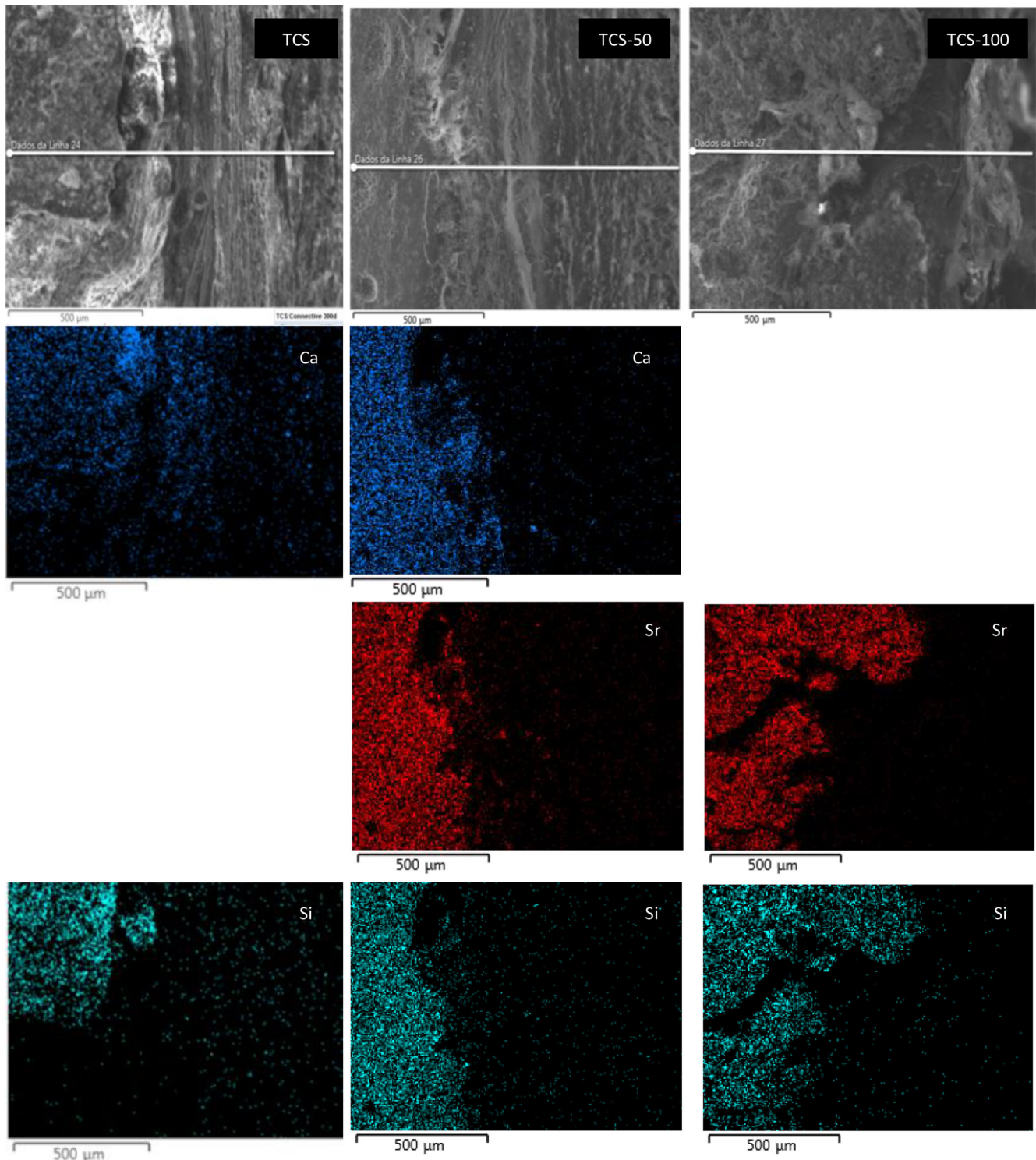
FIGURE 5   Elemental maps at the material to subcutaneous tissue interface for all test materials showing elemental migration after 30 days of contact ($n = 5$)

HA released low levels of ions. The leaching increased over the 6-month period. The tricalcium silicate leached relatively high levels of Ca which reduced with Sr doping. The doped silicates also leached very high levels of Sr. In comparison the 50% doping in HA led to the leaching of more Sr than the 100% HA after 30 days but this trend was reversed after 180 days. The Fuji IX leached Sr unlike the Chemfil material.

3.1.1 | Assessment of local tissue tolerance and elemental migration

Histological assessment
The subcutaneous tissue histological representative images for 30 and 180 days after the material implantation are shown in Figure 4A,B,
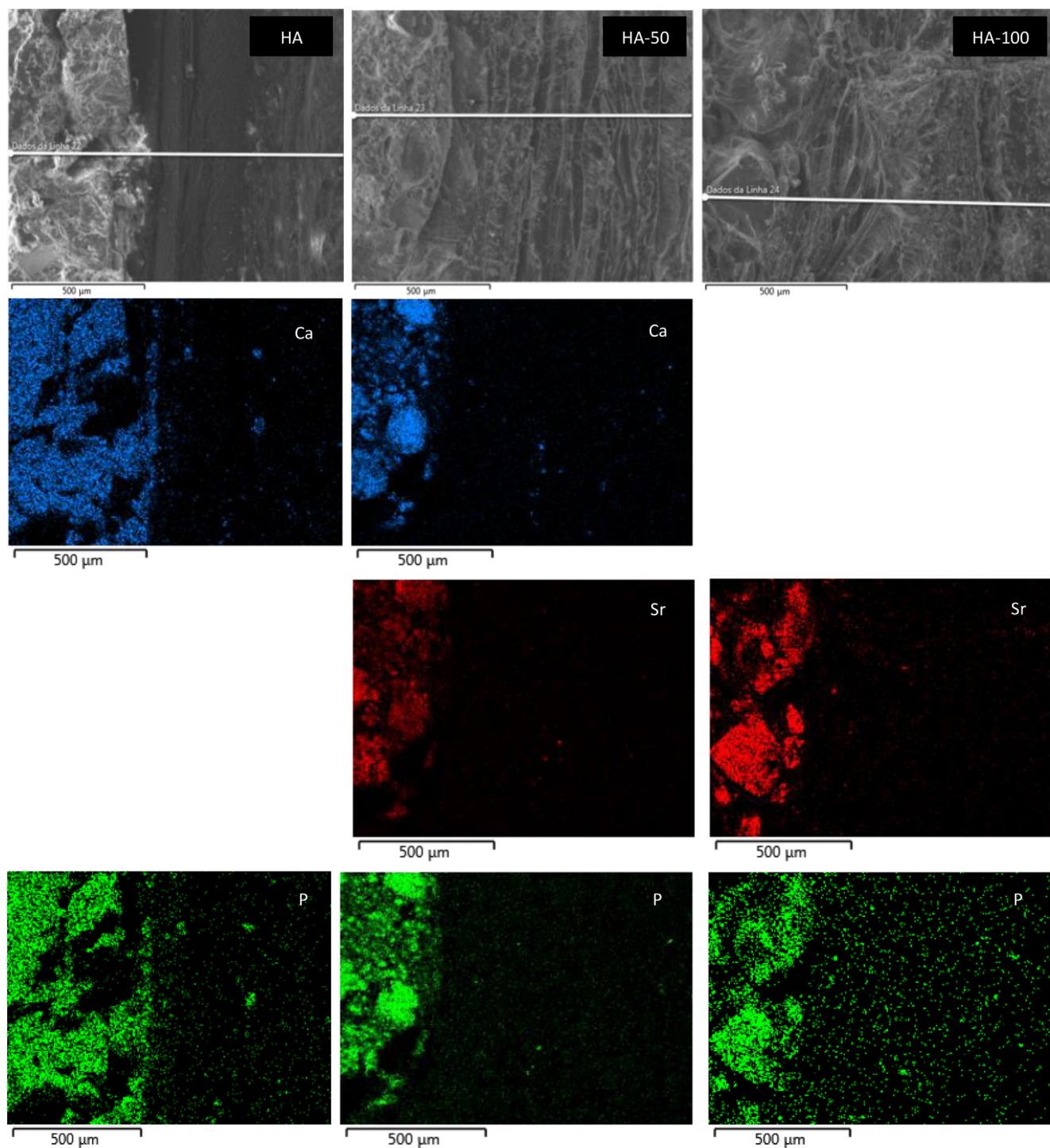
FIGURE 5 (Continued)

respectively. For three of the five animals in the TCS-100 group, the implanted material could not be located during the material retrieval procedures. Macroscopically, in the 30-day specimens, a thin layer of encapsulation was observed in the tissue surrounding the material implant with a perceptible increase in the encapsulation thickness after 180 days for all groups.

After 30 days in contact with the materials, the tricalcium silicate, hydroxyapatite, bioactive glass, and all the Sr-doped groups exhibited

moderate signs of tissue inflammation with inflammatory cells being present adjacent to the material implantation (red arrows in Figure 4A). Additionally, detached material fragments could be observed interposed within the connective tissue surrounded by a characteristic inflammatory chronic cell infiltrate representing a granulomatous foreign-body reaction (* in Figure 4A).

The glass ionomers induced an intense concentration of inflammatory cells largely distributed along the tissue to material interface
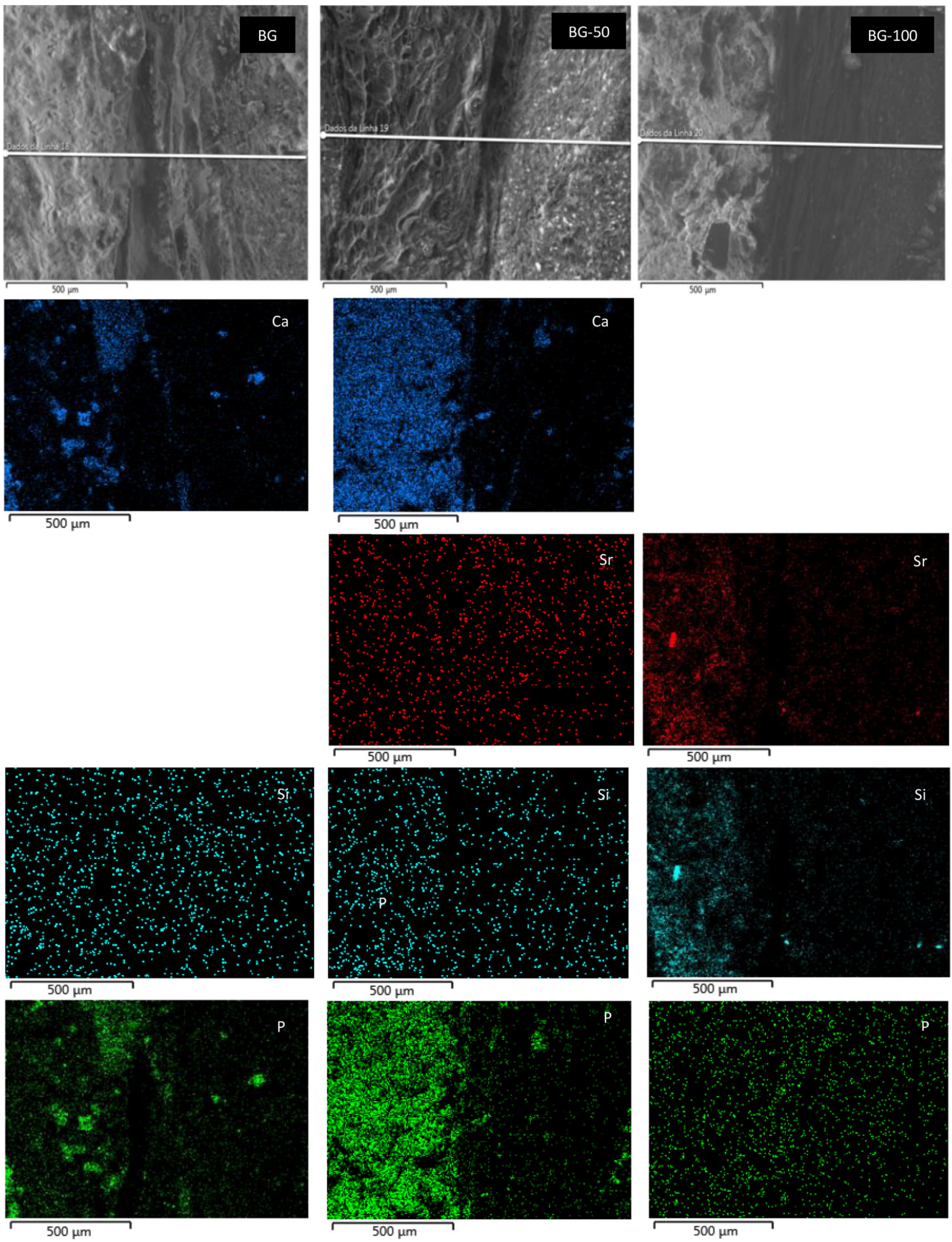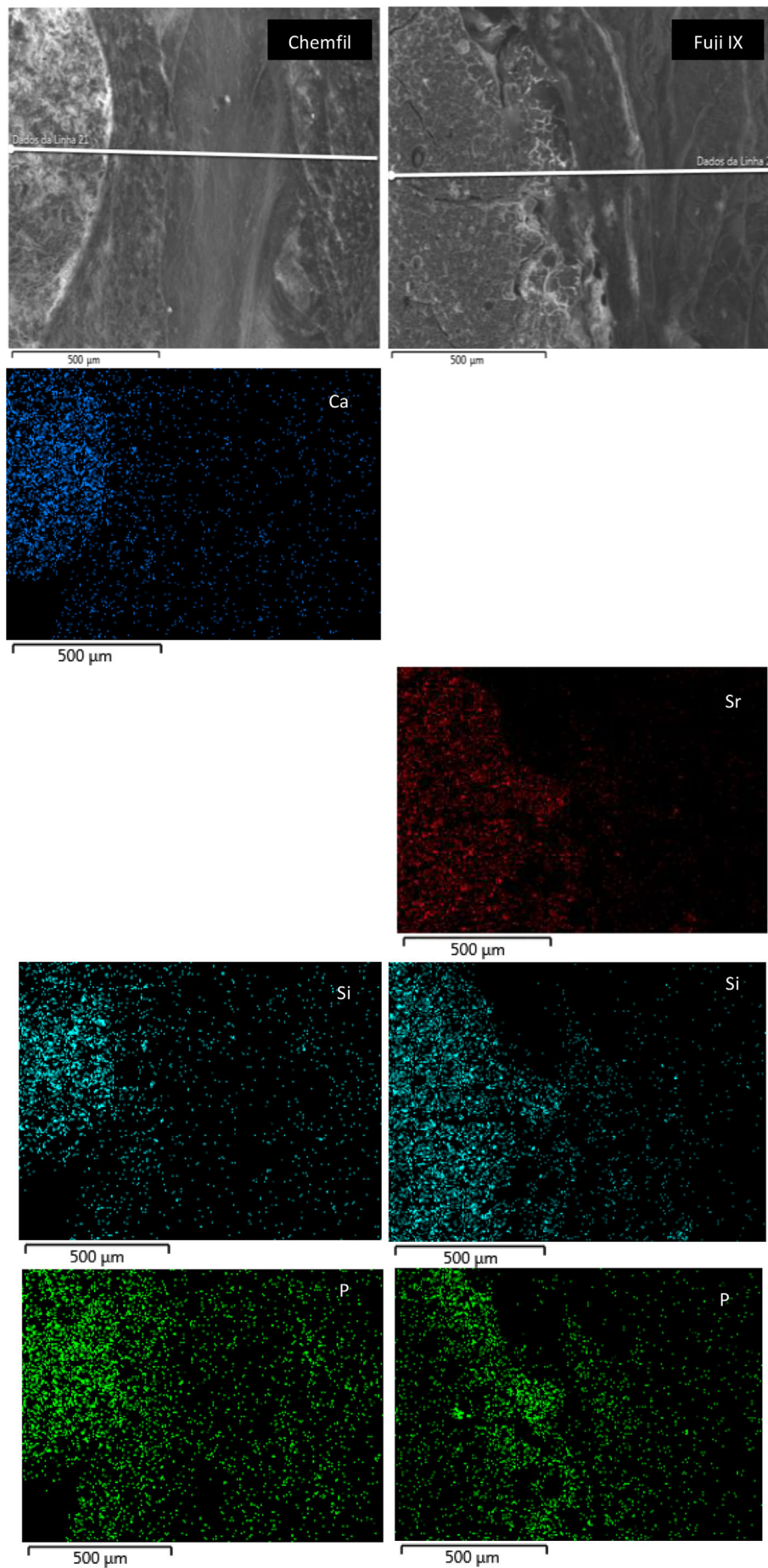
FIGURE 5 (Continued)
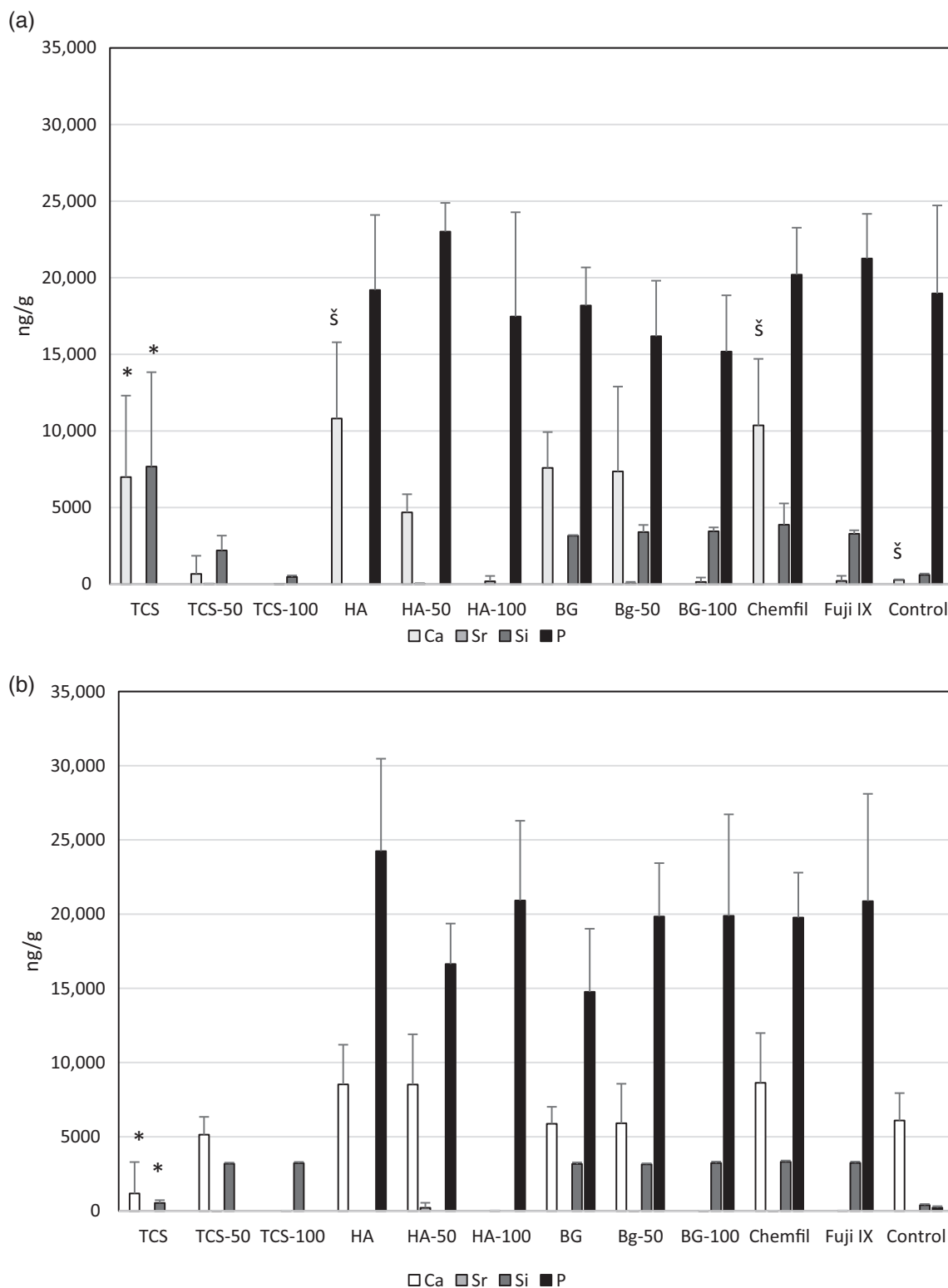
FIGURE 5 (Continued)

(a)

(b)

FIGURE 6 Levels of different elements detected after digestion of the tissues in contact with the materials (A) after 30 days and (B) after 180 days. The difference in the Ca and Si levels in TCS at 30 days and 180 days is marked with * and the higher level of Ca in HA and Chemfil compared to the control by š ($n = 5$)

with lymphocytes and multinucleated giant cells being evident (green arrows in Figure 4). The negative control exhibited relatively normal subcutaneous connective tissue histology without morphological alterations or inflammatory cells at both time periods.

After 180 days, the inflammatory reaction subsided, and tissue repair ensued with interposed stained collagen fibers being present (red arrows in Figure 4B). Some tissue disorganization (# in Figure 4B) could still be observed for all the 100% Sr-doped groups analyzed and
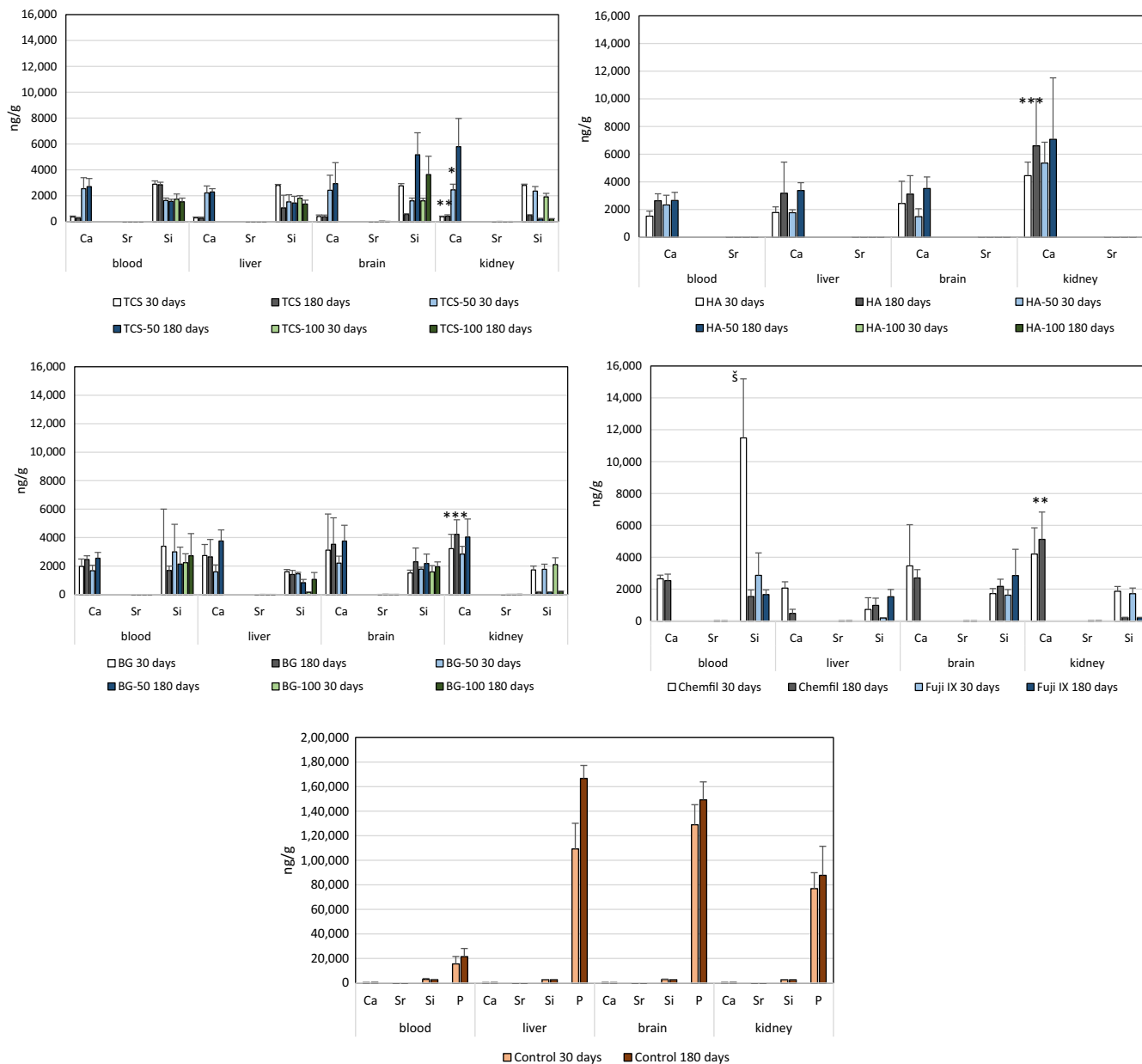
FIGURE 7   Peripheral elemental migration from the different test materials to different organs after 30 and 180-day subcutaneous implantation. The lower levels of calcium in the kidneys for TCS after 30 and 180 days and TCS-50 after 30 days compared with the other calcium containing material is indicated by *; The high level of silicon in the blood after 30 days for the ChemFil implantation is indicated by š ($n = 5$)

for the two commercial glass ionomers (Fuji and ChemFil) studied. Additionally, it was evident that there was moderate angiogenesis and mild fibrosis (§ Figure 4B) present for all implanted samples after this period of analysis.

Elemental migration assessment

The local elemental migration from the materials to the adjacent subcutaneous tissues is shown in Figure 5. The data for the elemental migration for the digested tissues in shown in Figure 6. The elemental maps show that the Sr was stable and bound to the material and this was confirmed by the analysis of the digested local tissues where the

level of Sr was relatively low compared with the other elements after both 30 and 180-day contact.

The Ca and Si presence in the tissues adjacent to the TCS is shown in the elemental map for TCS (Figure 5). By 180 days the Ca and Si could not be detected in the tissues (Figure 6A) and the level detected by the tissue digestion analysis exhibited lower levels after 180 days ($p < .05$). HA and Chemfil also exhibited high Ca levels in the tissues adjacent to the materials after 30 days of contact compared with the control ($p = .02$, $p = .039$, respectively). Phosphorus was detected in all materials known to contain P including the control (Figure 6). The presence of P in the tissue was also evident in the elemental maps (Figure 5).
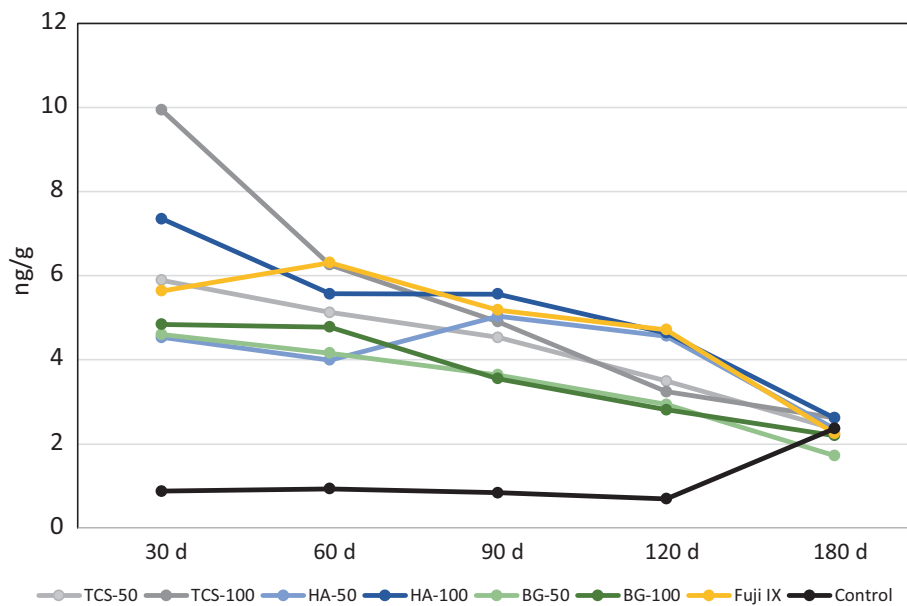
FIGURE 8 Strontium levels in the blood of test animals collected periodically over a period of 180 days after subcutaneous material implantation ($n = 5$)

The peripheral elemental migration analyses after 30 and 180-day contact in the cardiac blood and levels in the liver, brain and kidney are shown in Figure 7 including the control tissues. Analyses in the control animals showed high levels of P in all the peripheral organs so the P levels were omitted from the analysis of the test materials. The Sr levels in the cardiac blood and in the peripheral organs were negligible and similar to all materials and comparable with the control ($p > .05$). There was Ca retention in the kidneys for all materials except TCS after 30 days. After 180 days both TCS and TCS-50 had lower Ca levels than the other calcium containing materials ($p < .05$) with levels similar to the control ($p > .05$). The Si level in the cardiac blood for Chemfil was higher than the control and the other materials ($p < .001$). The level of Sr in the blood extracted at different intervals is shown in Figure 8. Following implantation of all Sr containing materials the presence of Sr in the blood was evident with the TCS-100 and HA-100 exhibiting the highest initial levels. All materials exhibited the same Sr level as the control after 180 days indicating the removal of the Sr from the peripheral blood.

4 | DISCUSSION

The current study investigated three material types namely bioactive glass, calcium phosphate and calcium silicates. The silicates and phosphates were mixed with water as reaction with water led to material hardening while the bioglass was mixed with sodium alginate and calcium chloride to allow its cross-linking. For all material subtypes, the Ca was substituted either partially or totally with Sr. Substitution of Ca with Sr has been investigated for bioactive glass and hydroxyapatite for medical applications and in glass ionomer cements in dentistry. Sr substituted hydraulic cements have not previously been investigated. The substitution of Ca with Sr has been shown to destabilize bioactive glass due to the larger atomic size of the Sr compared with Ca.[7] Due to this, leaching of Sr into solution occurs which was also

demonstrated in the current study. The most stable material was shown to be the HA as the substitution of the Ca in the calcium silicate structure led to the formation of multiple phases with a resultant high leaching.

Sr should not be of concern if leached as previous studies have indicated biocompatibility and osseointegration of various strontium doped materials.[31-33] Although leaching from bioactive materials is suggested to be beneficial as the ions interact with the tissues resulting in bioactivity, the materials sustain increased porosity and deterioration of the physical and mechanical properties over time. The leaching of Sr from the silicate cements was high and thus necessitated the investigation of the local and systemic effects of the leached Sr. Consequently, an animal model was employed and the materials were placed in direct contact with tissue. Subcutaneous direct implantation was used to give the worse-case scenario for elemental migration. This approach was used in a previous study[34] as it allowed direct tissue contact as occurs in a clinical situation.[26] With the exception of the Sr, the elements investigated are native to the human body thus levels of Ca and P in the control animals were also monitored. Elemental migration from dental cements has already been investigated using a similar animal model.[23-26] However, in the current study the implantations were not made in tubes to maximise contact of the materials with the tissues, no concerning lasting effects or elemental depositions were identified lasting apart from calcium in the kidneys.

Three of the five 100% Sr replaced silicate implants could not be retrieved after 180 days. If the materials are used clinically as resorbable materials, this would indicate that the material had been completely removed by the biological system. If used to replace missing structure, material dissolution can be of clinical concern. Previous studies have shown the loss of tricalcium silicate from the implantation site when used in an animal model.[34] The local tissue reactions for all materials included a moderate inflammatory response which subsided in the longer term. This finding was in accordance with previous studies using animal implantation for dental materials

evaluation.[35-37] The presence of newly formed blood vessels observed in the present study could increase blood circulation at the implantation site which may potentially result in further leaching and elemental migration to the peripheral organs.

The tricalcium silicate material had a local effect with migration of Ca and Si in the local tissues indicated in the elemental maps; however, while all the other materials led to calcium accumulation in the kidneys, the tricalcium silicate did not leave any traces. Tricalcium silicate is alkaline[38] and this may affect its relatively rapid metabolism of the material and its excretion from the body.

Regardless of the relatively high leaching of Sr from the silicate cements, there did not appear to be traces of Sr in the tissues and peripheral organs. The levels in the peripheral blood also reduced throughout the 180-day period and there also was no differential effects between the materials regardless of their leaching pattern.

The ion releasing capacity of glass ionomer cements is well reported. However the focus has previously been on the release of sodium fluoride and its anticariogenic properties as well as the replacement of Ca with the HA in the tooth structure and thus the effect on chemical bonding. The Fuji IX contains no Ca as it is a Sr replaced glass ionomer and previous studies conducted on this material indicated that Sr was not involved in the remineralization of carious lesions.[39] In fact, the Sr was quite stable and did not migrate along the tooth to material interface.[40,41] This was also consistent with the present study where even in the materials that released relatively high amounts of Sr, it did not migrate to the local tissues.

The current study also investigated Si migration as this has not yet been studied significantly in the biomedical field. Some reports have indicated that Si participates in the development and differentiation of connective tissue and that it can bind to a range of different elements.[42-44] The release of Si from hydraulic cements has been investigated[45,46] as has the migration to neighboring tissues[47,48] which was also shown in the current study. The control material also contained silicon in the tissues of the peripheral organs. Chemfil exhibited high levels of Si in cardiac blood and this may be a concern. The release of Si from glass ionomer cements has also been reported[49] but no correlation has been made with any toxic effects of this release. Interestingly, the synergistic effects of Sr and Si have been reported[50-53] and this requires further investigation for the further development of Si-based silicate cements.

5 | CONCLUSIONS

Strontium can replace calcium in bioactive materials. The replacement of calcium in silicate cements requires further investigation.

ORCID

Lauter Eston Pelepenko https://orcid.org/0000-0002-8365-8267
Thiago Bessa Marconato Antunes https://orcid.org/0000-0001-6594-3948
Elisa Boanini https://orcid.org/0000-0003-3754-0273
Josette Camilleri https://orcid.org/0000-0003-3556-6365

REFERENCES

1. Hench LL, Splinter RJ, Allen WC, Greenlee TK. Bonding mechanisms at the interface of ceramic prosthetic materials. *J Biomed Mater Res*. 1971;5:117-141.
2. Hench LL, Paschall HA. Direct chemical bond of bioactive glass-ceramic materials to bone and muscle. *J Biomed Mater Res*. 1973;7:25-42.
3. Bonnelye E, Chabadel A, Saltel F, Jurdic P. Dual effect of strontium ranelate: stimulation of osteoblast differentiation and inhibition of osteoclast formation and resorption in vitro. *Bone*. 2008;42:129-138.
4. Marie PJ, Hott M, Modrowski D, et al. An uncoupling agent containing strontium prevents bone loss by depressing bone-resorption and maintaining bone-formation in estrogen-deficient rats. *J Bone Miner Res*. 1993;8:607-615.
5. Gentleman E, Fredholm YC, Jell G, et al. The effects of strontium-substituted bioactive glasses on osteoblasts and osteoclasts in vitro. *Biomaterials*. 2010;31:3244-3252.
6. Fredholm YC, Karpukhina N, Law RV, Hill RG. Strontium containing bioactive glasses: glass struc- ture and physical properties. *J Non-Cryst Solids*. 2010;356:2546-2551.
7. Fredholm YC, Karpukhina N, Brauer DS, Jones JR, Law RV, Hill RG. Influence of strontium for calcium substitution in bioactive glasses on degradation, ion release and apatite formation. *J R Soc Interface*. 2012;9(70):880-889.
8. Moghanian A, Firoozi S, Tahriri M, Sedghi A. A comparative study on the in vitro formation of hydroxyapatite, cytotoxicity and antibacterial activity of 58S bioactive glass substituted by Li and Sr. *Mater Sci Eng C Mater Biol Appl*. 2018;91:349-360.
9. Bellucci D, Salvatori R, Anesi C, L2, Cannillo V. SBF assays, direct and indirect cell culture tests to evaluate the biological performance of bioglasses and bioglass-based composites: three paradigmatic cases. *Mater Sci Eng C Mater Biol Appl*. 2019;96:757-764.
10. Tripathi H, Rath C, Kumar AS, Manna PP, Singh SP. Structural, physico-mechanical and in-vitro bioactivity studies on SiO2-CaO-P2O5-SrO-Al2O3 bioactive glasses. *Mater Sci Eng C Mater Biol Appl*. 2019;94:279-290.
11. Bigi A, Boanini E. Functionalized biomimetic calcium phosphates for bone tissue repair. *J Appl Biomater Funct Mater*. 2017;15:e313-e325. doi:10.5301/jabfm.500036
12. Boanini E, Torricelli P, Fini M, Bigi A. Osteopenic bone cell response to strontium-substituted hydroxyapatite. *J Mater Sci Mater Med*. 2011;22:2079-2088.
13. Salamanna F, Giavaresi G, Parrilli A, et al. Antiresorptive properties of strontium substituted and alendronate functionalized hydroxyapatite nanocrystals in an ovariectomized rat spinal arthrodesis model. *Mater Sci Eng C Mater Biol Appl*. 2019;95:355-362.

14. Korovessis P, Mpountogianni E, Syrimpeis V, Baikousis A, Tsekouras V. Percutaneous injection of strontium containing hydroxyapatite versus Polymethacrylate plus short-segment pedicle screw fixation for traumatic A2- and A3/AO-type fractures in adults. *Adv Orthop*. 2018;2018:6365472-6365478.

15. Geng Z, Wang X, Zhao J, et al. The synergistic effect of strontium-substituted hydroxyapatite and microRNA-21 on improving bone remodeling and osseointegration. *Biomater Sci*. 2018;6(10):2694-2703.

16. Boanini E, Torricelli P, Sima F, et al. Gradient coatings of strontium hydroxyapatite/zinc β-tricalcium phosphate as a tool to modulate osteoblast/osteoclast response. *J Inorg Biochem*. 2018;183:1-8.

17. Simila HO, Karpukhina N, Hill RG. Bioactivity and fluoride release of strontium and fluoride modified biodentine. *Dent Mater*. 2018;34(1):e1-e7.

18. Alhashimi RA, Mannocci F, Sauro S. Bioactivity, cytocompatibility and thermal properties of experimental bioglass-reinforced composites as potential root-canal filling materials. *J Mech Behav Biomed Mater*. 2017;69:355-361.

19. Hoikkala NJ, Wang X, Hupa L, Smått JH, Peltonen J, Vallittu PK. Dissolution and mineralization characterization of bioactive glass ceramic containing endodontic sealer Guttaflow bioseal. *Dent Mater J*. 2018;37(6):988-994.

20. Santos JM, Pereira S, Sequeira DB, et al. Biocompatibility of a bioceramic silicone-based sealer in subcutaneous tissue. *J Oral Sci*. 2019;61(1):171-177.

21. Rodríguez-Lozano FJ, Collado-González M, Tomás-Catalá CJ, et al. GuttaFlow bioseal promotes spontaneous differentiation of human periodontal ligament stem cells into cementoblast-like cells. *Dent Mater*. 2019;35(1):114-124.

22. Huang M, Hill RG, Rawlinson SC. Strontium (Sr) elicits odontogenic differentiation of human dental pulp stem cells (hDPSCs): a therapeutic role for Sr in dentine repair? *Acta Biomater*. 2016;38:201-211.

23. Demirkaya K, Demirdöğen BC, Torun ZÖ, Erdem O, Çırak E, Tunca YM. Brain aluminium accumulation and oxidative stress in the presence of calcium silicate dental cements. *Hum Exp Toxicol*. 2017;36(10):1071-1080.

24. Demirkaya K, Can Demirdöğen B, Öncel Torun Z, Erdem O, Çetinkaya S, Akay C. In vivo evaluation of the effects of hydraulic calcium silicate dental cements on plasma and liver aluminium levels in rats. *Eur J Oral Sci*. 2016;124(1):75-81.

25. Garcia LDFR, Huck C, Magalhães FAC, Souza PPC, Souza Costa CA. Systemic effect of mineral aggregate-based cements: histopathological analysis in rats. *J Appl Oral Sci*. 2017;25(6):620-630.

26. Simsek N, Bulut ET, Ahmetoğlu F, Alan H. Determination of trace elements in rat organs implanted with endodontic repair materials by ICP-MS. *J Mater Sci Mater Med*. 2016;27(3):46.

27. Khalil WA, Eid NF. Biocompatibility of BioAggregate and mineral trioxide aggregate on the liver and kidney. *Int Endod J*. 2013;46(8):730-737.

28. National Academies Press. *Guide for the Care and Use of Laboratory Animals*. National Academies Press; 2011.

29. Faul F, Erdfelder E, Lang AG, Buchner A. G*power 3: a flexible statistical power analysis program for the social, behavioral, and biomedical sciences. *Behav Res Methods*. 2007;39:175-191.

30. Cohen J. *Statistical Power Analysis for the Behavioral Sciences*. 2nd ed. Lawrence Erlbaum Associates; 1988.

31. Zhang S, Dong CYM, Xu Y, Ping J, Chen W, Liang W. Recent developments in strontium-based biocomposites for bone regeneration. *J Artif Organs*. 2020;23:191-202.

32. Basu B, Sabareeswaran A, Shenoy SJ. Biocompatibility property of 100% strontium-substituted SiO_2-Al_2O_3-P_2O_5-CaO-CaF_2 glass ceramics over 26 weeks implantation in rabbit model: histology and micro-computed tomography analysis. *J Biomed Mater Res B Appl Biomater*. 2015;103(6):1168-1179.

33. Sabareeswaran A, Basu B, Shenoy SJ, Jaffer Z, Saha N, Stamboulis A. Early osseointegration of a strontium containing glass ceramic in a rabbit model. *Biomaterials*. 2013;34(37):9278-9286.

34. Wismayer PS, Lung CYK, Rappa F, Cappello F, Camilleri J. Assessment of the interaction of Portland cement-based materials with blood and tissue fluids using an animal model. *Sci Rep*. 2016;6:34547.

35. Zhang W. Peng B tissue reactions after subcutaneous and intraosseous implantation of iRoot SP, MTA and AH plus. *Dent Mater J*. 2015;34:774-780.

36. Tavares CO, Böttcher DE, Assmann E, et al. Tissue reactions to a new mineral trioxide aggregate-containing endodontic sealer. *J Endod*. 2013;39:653-657.

37. Scarparo RK, Haddad D, Acasigua GAX, Fossati ACM, Fachin EVF, Grecca FS. Mineral trioxide aggregate-based sealer: analysis of tissue reactions to a new endodontic material. *J Endod*. 2010;36:1174-1178.

38. Camilleri J. Characterization and hydration kinetics of tricalcium silicate cement for use as a dental biomaterial. *Dent Mater*. 2011;27:836-844.

39. Kim YK, Yiu CK, Kim JR, et al. Failure of a glass ionomer to remineralize apatite-depleted dentin. *J Dent Res*. 2010;89(3):230-235.

40. Dabsie F, Gregoire G, Sixou M, Sharrock P. Does strontium play a role in the cariostatic activity of glass ionomer? Strontium diffusion and antibacterial activity. *J Dent*. 2009;37(7):554-559.

41. Moheet IA, Luddin N, Ab Rahman I, et al. Analysis of ionic-exchange of selected elements between novel Nano-hydroxyapatite-silica added glass ionomer cement and natural teeth. *Polymers*. 2021;13(20):3504.

42. Pietak AM, Reid JW, Stott MJ, Sayer M. Silicon substitution in the calcium phosphate bioceramics. *Biomaterials*. 2007;28:4023-4032.

43. Henstock JR, Canham LT, Anderson SI. Silicon: the evolution of its use in biomaterials. *Acta Biomater*. 2015;11:17-26. doi:10.1016/j.actbio.2014.09.025

44. Jurkić LM, Cepanec I, Pavelić SK, Pavelić K. Biological and therapeutic effects of ortho-silicic acid and some ortho-silicic acid-releasing compounds: new perspectives for therapy. *Nutr Metab*. 2013;10:2.

45. Arias-Moliz MT, Farrugia C, Lung CYK, Wismayer PS, Camilleri J. Antimicrobial and biological activity of leachate from light curable pulp capping materials. *J Dent*. 2017;64:45-51.

46. Koutroulis A, Kuehne SA, Cooper PR, Camilleri J. The role of calcium ion release on biocompatibility and antimicrobial properties of hydraulic cements. *Sci Rep*. 2019;9(1):19019.

47. Kebudi Benezra M, Schembri Wismayer P, Camilleri J. Interfacial characteristics and Cytocompatibility of hydraulic sealer cements. *J Endod*. 2018;44(6):1007-1017.

48. Viapiana R, Guerreiro-Tanomaru J, Tanomaru-Filho M, Camilleri J. Interface of dentine to root canal sealers. *J Dent*. 2014;42(3):336-350.

49. Roussou K, Nikolaidis AK, Ziouti F, Arhakis A, Arapostathis K, Koulaouzidou EA. Cytotoxic evaluation and determination of organic and inorganic eluates from restorative materials. *Molecules*. 2021;26(16):4912.

50. Zhang W, Huang D, Zhao F, et al. Synergistic effect of strontium and silicon in strontium-substituted sub-micron bioactive glass for enhanced osteogenesis. *Mater Sci Eng C Mater Biol Appl*. 2018;89:245-255.

51. Wagner AS, Schumacher M, Rohnke M, et al. Incorporation of silicon into strontium modified calcium phosphate bone cements promotes osteoclastogenesis of human peripheral mononuclear blood cells. *Biomed Mater*. 2019;14:025004.

52. Roohaniesfahani I, Wang J, No YJ, de Candia C, et al. Modulatory effect of simultaneously released magnesium, strontium, and silicon ions on injectable silk hydrogels for bone regeneration. *Mater Sci Eng C Mater Biol Appl*. 2019;94:976-987.

53. Xing M, Wang X, Wang E, Gao L, Chang J. Bone tissue engineering strategy based on the synergistic effects of silicon and strontium ions. *Acta Biomater*. 2018;72:381-395.